ASSESSMENT OF THE ON-GROUND RISK DURING RE-ENTRIES

H. Klinkrad

Mission Analysis Section, ESA/ESOC, D-64293 Darmstadt, Germany

ABSTRACT

The present paper outlines methods which allow to quantify and monitor the on-ground population risk in the course of a hazardous re-entry event. The risk potential will be derived from an object related casualty cross-section, the endangered ground swath, and the underlying population density. Means will be described to perform a long-term risk assessment for a given latitude band, and a short-term risk assessment for a given nodal longitude of the final re-entry orbit. In case of residual manoeuvring capabilities strategies will be outlined to manage and reduce the risk potential by controlling the nodal longitude of the final orbit, and the impact footprint. The usefulness of these concepts will be demonstrated for the historic re-entries of Skylab and Salyut-7, and for the recent re-entry of the Mir space station.

1. INTRODUCTION

Of the 26,500 Earth orbiting objects which USSPACECOM has tracked since 1957 more that 18,000 have re-entered into the atmosphere by the year 2001. Most of these objects disintegrated and burnt up, posing only a minor risk on ground. In the year 2001 the number of unclassified, correlated objects in the USSPACECOM catalog was on the order of 8,500. Due to the limited sensor sensitivities, all of these objects have diameters larger than 10 to 30 cm. Out of the catalog population, about 1 object re-enters each day, and 1 to 2 objects with a radar cross-section (RCS) larger than 1 m^2 re-enter each week. The latter ones, which have a radius of about 1 m, have an increased survival potential, and they are generally followed more closely by USSPACECOM until their final entry. A NASA [4] analysis of several months of such re-entry monitoring and prediction exercises indicated that the global distribution of entry locations, for the given inclination distribution of the catalog orbits, is rather uniform, with no evident clustering on the Northern or Southern hemisphere.

Occasionally, at rates of one in several years orbital structures re-enter, which have geometric cross-sections of 100 m^2 or more, and masses of several 10 tons. Such spacecraft can be classified as high-risk objects, since they produce a significant mass percentage of break-up fragments which can withstand the aerothermal heat flux and structural loads during re-entry, and which can generate ground impacts with significant risk levels to the population within the debris swath. Historic examples of this category were the re-entries of Skylab (on 11-Jul-1979, with a mass of 74 t), and Salyut-7 (on 07-Feb-1991, with a mass of 40 t). The latest, most massive object in space history to re-enter was Mir (on 23-Mar-2001, with a mass of 135 t). The re-entry of Skylab was analysed in detail by Dreher [2] et al., while the Salyut-7 event was well documented in the proceedings of an ESOC workshop [5]. Results of re-entry simulations with satellite break-up models were compiled by Fritsche [3] et al., and by Bouslog [1] et al. In context with launch events, Kompaniets [8] et al., and Smith [11] investigated possible debris sources, and derived related on ground risks. Based on available technical information, NASA [10], ESA [6], and NASDA compiled debris mitigation handbooks, which also address risk assessment and mitigation procedures for uncontrolled re-entries.

In the present paper the risk associated with the re-entry of a risk object will be analysed, based on empirically justified and computationally verified assumptions on the break-up altitude, and on the cross track and along track extension of an impact probability distribution. The most prominent historic re-entries of massive objects, i.e. the decays of Skylab, Salyut-7, and Mir, will be used to discuss results of the risk analysis methods which are developed in this paper.

2. RE-ENTRY GROUND SWATH

Some 80% of the currently catalog space object population have near-circular orbits of $e < 0.05$. This is partly due to operational practices, and partly due to the natural circularisation of orbits under the effect of airdrag, concentrated around perigee passes. Those orbits which due not fall under this category are mostly highly eccentric throughout their orbital lifetime, with their decays driven by luni-solar perturbations acting on the perigee altitude. Such re-entries can be forecast with good precision, and they will not be dealt with in this paper. The dominant class of near-circular orbits shows clusters at certain inclination bands. The orbital inclinations are very stable

Proceedings of the 3rd European Conference on Space Debris, ESOC, Darmstadt, Germany, 19 - 21 March 2001
(ESA SP-473, August 2001)

during the entire orbital phase, and they can be used for a coarse risk analysis, focused on the constrained latitude band of $\phi \in [-i, +i]$.

impact probability	1σ	2σ	3σ
elliptic corridor	0.39347	0.86466	0.98889
rectangular corridor	0.46606	0.91107	0.99987

Tab. 1: Integrated impact probability for elliptic and rectangular fragment dispersion areas of 1σ, 2σ, and 3σ extensions along track and cross track.

The prediction of the orbital decay of a spacecraft, and of its final re-entry, aerothermal break-up, and ground dispersion of fragments is affected by uncertainties of the initial orbit and attitude state, of the ambient atmosphere, of the aerodynamic characteristics, of the structural and thermal response of the materials, and of the resulting break-up altitude and fragment spread. Depending on the entry angle and break-up altitude, the ground dispersion of fragments can extend over more than ±1500 km along track and ±80 km cross track, assuming a sustained lift-to-drag ratio of up to $L/D \approx 1$, and a mean break-up altitude of 80 km. During the orbital decay phase, the final re-entry location can only be predicted with considerable uncertainties, which can be cumulated into an impact probability density function (PDF). This PDF can be formally produced by propagating the overall error covariance matrix from the last available orbit determination to the most probable re-entry location, which shall be denoted as the centre of impact window (COIW). Based on the analysis of 15 historic re-entry events, we shall assume that the 2σ extension of the fragment dispersion area on ground is an ellipse, which is symmetric to the predicted COIW location, both in the along and cross track direction. We shall further assume that the along track extension corresponds to a ±20% error in the COIW time, and that the cross track extension is ±80 km, relative to a drift corrected ground track. For implementation purposes, we shall analyse a rectangular fragment dispersion area which is tangent to the 2σ dispersion ellipse. The resulting probabilities of an impact within a 1σ, 2σ, and 3σ ellipse and rectangle are listed in Tab.1. For the adopted conditions, the total impact probability within a 2σ rectangular ground swath is 91.1% (as compared to 86.5% for the elliptic integration limits).

$\Delta t_{pred}(d)$	$\sum_i^n \Delta t_N(sec)$	$\sum_i^n \Delta\lambda_N(°)$	$\sum_i^n \Delta s_u(km)$
10.0	1,052	4.39	7,895
5.0	266	1.11	1,997
1.0	12	0.05	87

Tab. 2: Groundtrack drift due to cumulated changes Δt_N in nodal period, and their effect on nodal longitude $\Delta\lambda_N$, and along track position Δs_u, as a function of the time span Δt_{pred} (Mir orbit at $i = 51.6°$ and $H = 200$km).

In the course of a re-entry prediction campaign the reference 2σ ground swath can experience considerable drifts in longitude, depending on the offset of the current COIW prediction relative to the final re-entry epoch. These drifts must be taken into consideration, since they may be of comparable magnitudes as the adopted 2σ cross track swath extension. A detailed description of the groundtrack adjustment procedure is provided by Klinkrad [7].

Tab.2 summarises related results for the Mir groundtrack drift (inclination 51.6°, with decay to an altitude of 200 km at the end of the propagation). In all analysed cases the application of the groundtrack correction scheme to previously predicted COIW locations led to an adjusted cross-track position well within ±5 km of the most recent prediction.

3. CASUALTY CROSS-SECTION

One of the key issues in re-entry risk analyses is the identification of components of a spacecraft which are likely to survive the deceleration and heating peaks following a break-up event at altitudes of typically 75 to 80 km. Studies sponsored by NASA [1] and ESA [3] have addressed this challenging task, which involves a simultaneous solution of 6 degrees-of-freedom (DoF) flight dynamics equations, with aerodynamic, aerothermodynamic, thermal, and structural loads acting on a complicated geometry, composed of many different materials. Computations predict that certain materials (e.g. stainless steel), and certain shapes (e.g. tanks) have a particularly good potential of re-entry survival, particularly if high melting temperatures are combined with low area-to-mass ratios. The retrieval of such objects at several re-entry sites has supported these assumptions [2, 4].

In order to assess the on-ground risk due to surviving debris of a single re-entry event, the NASA safety standard [10] NSS 1740.14 introduces an equivalent casualty cross-section A_c, which is composed of the cross-sections A_i of individual fragments, augmented by a projected human risk cross-section of $A_h = 0.36\text{m}^2$ (corresponding to $\sqrt{A_h} = 0.6$m, as used by NASA).

$$A_c = \sum_{i=1}^{n} \left(\sqrt{A_h} + \sqrt{A_i} \right)^2 \qquad (1)$$

This quantity A_c is a simple, yet very efficient way to concentrate the entire knowledge on the break-up process of a re-entering spacecraft into a single figure. It would allow a spacecraft manufacturer to provide means for a reliable re-entry risk assessment without disclosing sensitive information on construction details. As such, the casualty cross-section could become a common international standard of data exchange in the course of re-entry prediction campaigns (e.g. in the frame of the Inter-Agency Space Debris Coordination Committee, IADC).

Using information from ESA's DISCOS database, 17,620 re-entry objects could be identified for the time span 1957 to 2001. 5,900 of them had information on their mean geometric cross-section A: 365 objects with $A > 20\text{m}^2$, 2,287 objects with $10\text{m}^2 < A < 20\text{m}^2$, 1,018 objects with $5\text{m}^2 < A < 10\text{m}^2$, 1,788 objects with $1\text{m}^2 < A < 5\text{m}^2$, and 12,162 objects with $A < 1\text{m}^2$ (including 11,725 with no information available). The resulting average cross-section is about $A = 5\text{m}^2$. When applying this value to eq.1, the effective mean casualty cross-section would be $A_c = 8\text{m}^2$ (the generating and dissipating effects from break-up and burn-up were not considered in the coarse assessment). This figure of $A_c = 8\text{m}^2$ happens to be identical to NASA's recommendation of a casualty cross-section threshold [10].

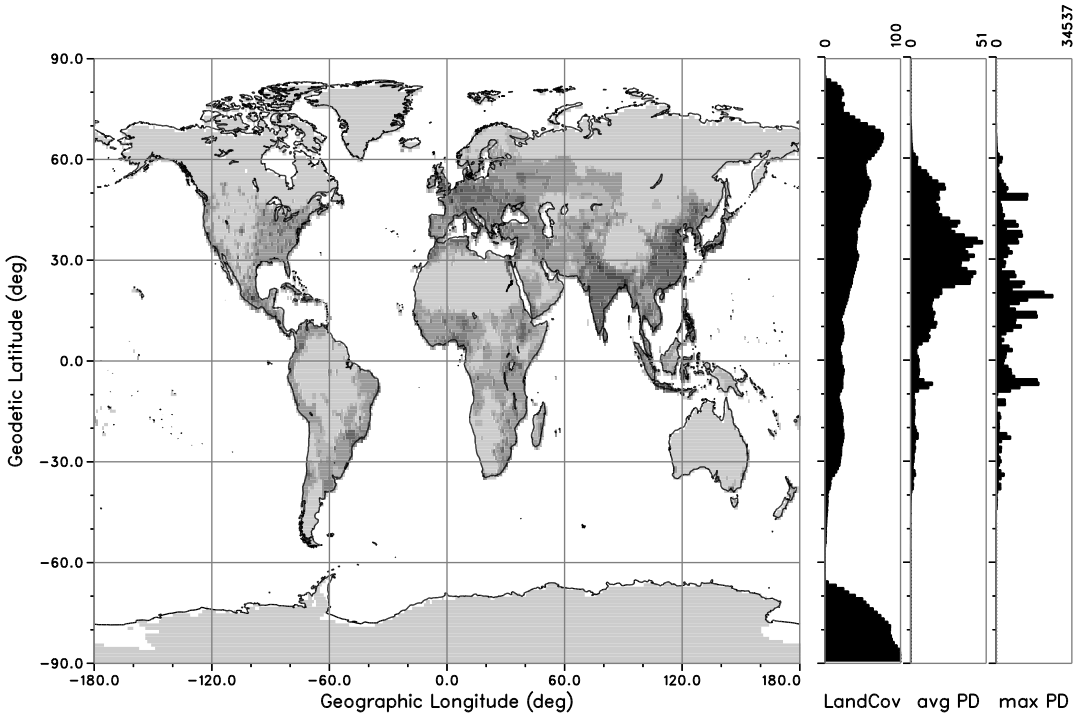

Fig. 1: World population density ($1° \times 1°$ cells). The small circle of latitude average of land cover (in %), and of the mean and maximum population density (in $1/\text{km}^2$) is given to the right.

4. POPULATION DENSITY

Population density maps with sufficient spatial resolution are necessary to associate the impact of re-entry survivor objects with a casualty risk in the affected groundtrack swath. Fig.1 shows a world map of $1° \times 1°$ mean population densities, derived from 5' × 5' (9.25km × 9.25km) high resolution data of the Global Demography Project [9]. These population data for the year 1994 are supported by discretised maps of land masses.

	$\rho_p, 1/\text{km}^2$	P_c for $A_c = 8\text{m}^2$
Earth, global/land	12.2/42.1	1:8,137/1:2,375
S.Hem., global/land	2.9/14.9	1:34,965/1:6,693
N.Hem., global/land	21.6/55.8	1:4,638/1:1,792

Tab. 3: Mean population densities of the Earth, and of its southern and northern hemisphere, with resulting impact casualty probabilities (for $A_c = 8\text{m}^2$, global means/means over land masses).

The total world population in 1994 was $5.63 \times 10^{+9}$, distributed over a total land surface of $1.48 \times 10^{+8}\,\text{km}^2$, which accounts for 28.97% of the surface of the Earth reference ellipsoid. This corresponds to a global mean population density of $11.0/\text{km}^2$, and to a mean land population density of $38.1/\text{km}^2$. The global maximum of the population density in 1994 (averaged over the 5' × 5' bin size) was $34537.0/\text{km}^2$, in the area of Bombay/India. By the year 2000, the world population had reached $6.23 \times 10^{+9}$. This value is predicted to double within the next 39 years.

The histograms on the right hand side of Fig.1 give the small circle of latitude averages of land cover (in %) and average population density (per km^2), plus the maximum density in each latitude band of 1° width. An imbalance between the northern and southern hemisphere becomes evident from these charts. In fact, only 11.7% of the world population, and only 33.3% of the land masses are located south of the equator. This has a direct impact on an equally imbalanced risk distribution between the hemispheres, with a much higher risk of re-entry casualties at northern latitudes (see Tab.3 and Fig.3).

5. LONG TERM RISK ASSESSMENT

The probability $P_i(\phi)$ that an uncontrolled re-entry from a near circular orbit of inclination i occurs in a certain latitude band at $\phi \leq i$ can be assessed by means of analytical equations (see [6]), assuming that for long-term risk forecasts the impact probability distribution in geographic longitude λ is uniform, and the orbital inclination remains stable.

The analytical assessment of $P_i(\phi)$ matches well with a corresponding graphs in Fig.2, which was produced by numerical integration along groundtracks of orbits with inclinations of 5.0° (e.g. Beppo-SAX), 28.5° (e.g. Shuttle payloads), 51.6° (e.g. Skylab, Salyut-7, Mir), 65.0° (e.g. Kosmos 954 and 1402), and 98.5° (sun-synchronous

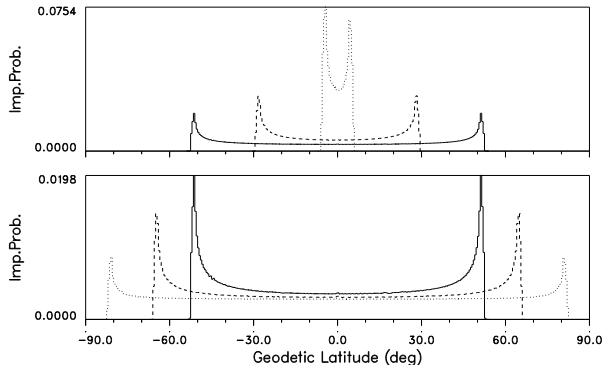

Fig. 2: Impact probability as a function of latitude (0.5° bins), for orbit inclinations 5.0° (top, dotted), 28.5° (top, dashed), 51.6° (top/bottom, solid line), 65.0° (bottom, dashed), and 98.5° (bottom, dotted).

orbits), for a latitude bin width of $\Delta\phi = 0.5°$. In order to link ground impact probability with local land coverage and population density, single orbit arcs were produced in steps of argument of true latitude of $\Delta u = 1°$, and in steps of geographic longitude of ascending node of $\Delta\lambda_n = 1°$ (for $\lambda_n \in [-180°, +180°]$). For each orbit arc the underlying maps of land masses and population densities were sampled, weighted with the resident probabilities, and assigned to bins of latitude ϕ (for Fig.3), bins of nodal longitude λ_n (for Fig.4), and (u,λ_n)-bins (for Fig.5).

Inclination	P_l	P_c
5.0 °	0.2315	0.562×10^{-4}
28.5 °	0.2732	1.403×10^{-4}
51.6 °	0.2728	1.314×10^{-4}
65.0 °	0.2877	0.982×10^{-4}
98.5 °	0.3333	0.844×10^{-4}

Tab. 4: Land impact probability P_l, and casualty probability P_c (assuming a 10 m^2 casualty cross-section), as a function of the orbit inclination.

According to Fig.2, the highest impact probability $P_i(\phi)$ can be expected close to the extreme latitudes, where $\phi \approx \pm i$. Since the integral value over all latitude bands is 1 by definition, the peak probability of $P_i(\phi)$ increases with decreasing inclination. After weighting of P_i with underlying land masses, the resulting land impact probability P_l shows a strong latitude asymmetry, as could be expected from Fig.1. This imbalance towards the northern hemisphere is further emphasised after weighting of P_i with local population densities to obtain a casualty risk probability P_c. Tab.4 summarises the global land impact probabilities P_l and casualty probabilities P_c for orbits of different inclinations (for an assumed spacecraft casualty cross-section of $A_c = 10\text{m}^2$). The highest land impact probability is noted for $i = 65°$, while the largest mean casualty risk is encountered on orbits of $i = 28.5°$.

Fig.4 shows land impact probability and casualty risk results, averaged over single orbit arcs, as a function of the geographic longitude of the ascending node λ_n, for the previous orbit inclinations. A clear concentration of casualty risk at certain values of λ_n is noticeable. This

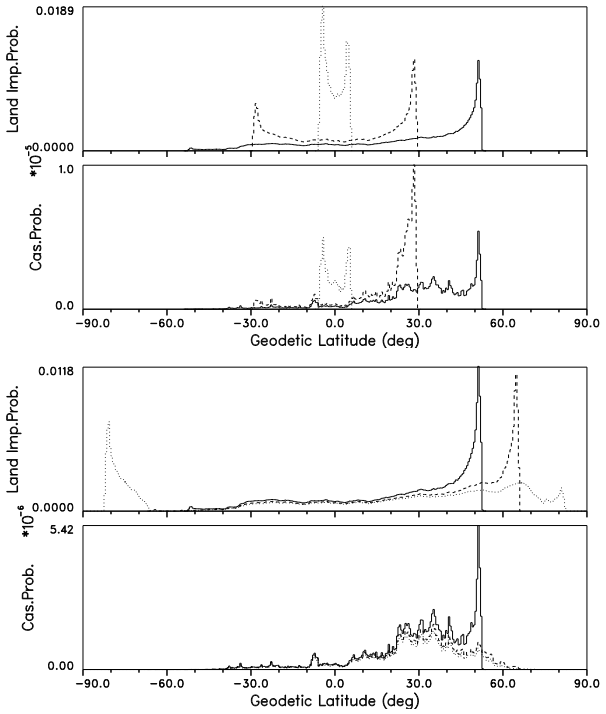

Fig. 3: Land impact, and casualty probability as a function of latitude (0.5° bins), for orbit inclinations 5.0° (top, dotted), 28.5° (top, dashed), 51.6° (top/bottom, solid line), 65.0° (bottom, dashed), and 98.5° (bottom, dotted).

knowledge can be used to target re-entry orbits towards longitudes of minimum risk, if the spacecraft has a residual manoeuvring capability (as was the case for Skylab). With decreasing orbital inclination, the land impact and casualty probability functions P_l and P_c tend to flatten out (note the different scales in the top and bottom set of charts of Fig.4), and the risk reduction effect from targeting to certain nodal longitudes is reduced.

6. NEAR TERM RISK ASSESSMENT

When the predicted orbital lifetime t_L of an uncontrolled re-entry drops below a few days, a more detailed risk prognosis becomes necessary. In this case, the previously adopted, drift corrected 2σ ground impact corridor (of $\pm$80 km width and of an along track extension corresponding to a time window of $\pm 0.2 t_L$) needs to be analysed with the proper weighting by a 2D impact probability density function ($PDF_{2\sigma}$). The general form of $PDF_{n\sigma}$ for an n_σ probability is

$$PDF_{n\sigma} = \frac{n_\sigma^2}{2\pi s_{x,n\sigma}\, s_{y,n\sigma}} \exp\left(-\frac{1}{2}\left(\frac{\Delta s_x^2}{s_{x,n\sigma}^2} + \frac{\Delta s_y^2}{s_{y,n\sigma}^2}\right)\right) \quad (2)$$

where s_x and s_y are the along track and cross track dimensions of the ellipse, $n_\sigma = 2$ for the adopted 2σ confidence level, $s_{x,n\sigma} = s_{x,2\sigma}$ and $s_{y,n\sigma} = s_{x,2\sigma}$ are the semi axes of this ellipse, centred on the COIW location, and Δs_x and Δs_y are the along track and cross track offsets from the predicted centre of the impact window (COIW).

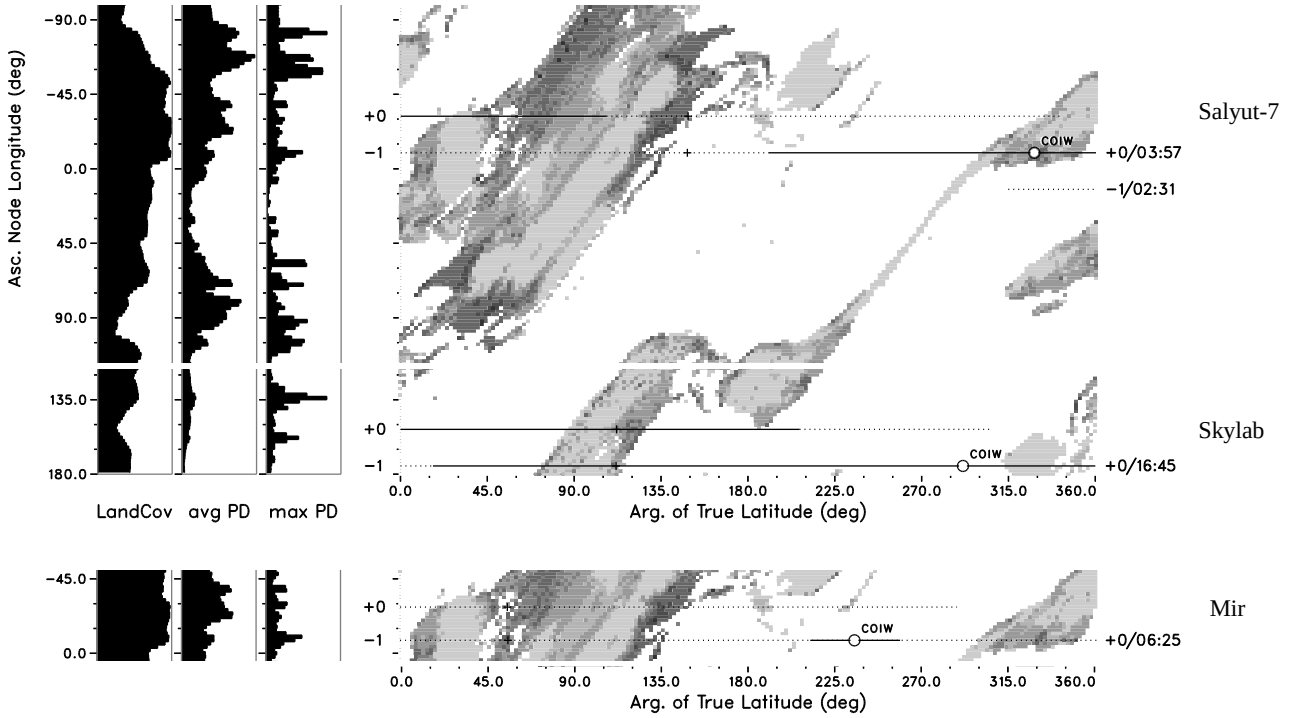

Fig. 5: Skylab, Salyut-7, and Mir re-entry groundtracks on a world population density map as a function of the geographic longitude of the ascending node λ_n, and of the orbit position (argument of true latitude u). The argument of true latitude average of land cover (in %), and mean and max. population density (per km^2) is given to the left.

A detailed risk analysis shall be performed by means of discretisation techniques, with the aim to replace integral expressions by finite summations. The spatial resolution on ground shall comply with the 9.25km × 9.25km resolution of the world population maps. For the forthcoming analysis, the ground swath information bins (of impact probability, land coverage, population density) shall be sampled at constant increments of $\delta s_x = 10$km along track, and $\delta s_y = 10$km cross track, over the rectangular swath area of 2σ extension (clipping of bins at the 2σ swath borders is applied). By approximation of the 2-dimensional, 2σ probability density integrals via finite summations one obtains the following results for the impact probability $P_{i,2\sigma}$, the land impact probability $P_{l,2\sigma}$, and the probability of population casualties $P_{c,2\sigma}$ for any given re-entry event.

$$P_{i,2\sigma} = \sum_{n=1}^{N} \sum_{m=1}^{M} (P_{i,2\sigma})_{n,m} \quad (3)$$

$$P_{l,2\sigma} = \sum_{n=1}^{N} \sum_{m=1}^{M} (P_{i,2\sigma})_{n,m} \times (\bar{f}_l)_{n,m} \quad (4)$$

$$P_{c,2\sigma} = \sum_{n=1}^{N} \sum_{m=1}^{M} (P_{i,2\sigma})_{n,m} \times (\bar{\rho}_p)_{n,m} \times A_c \quad (5)$$

where the local impact probability is defined as

$$(P_{i,2\sigma})_{n,m} = PDF_{2\sigma}(\Delta s_{xn}, \Delta s_{y_m}) \times \delta s_x \times \delta s_y \quad (6)$$

$(\bar{f}_l)_{n,m}$ is the fraction of land coverage, and $(\bar{\rho}_p)_{n,m}$ is the average population density in the sampled ground swath area bin, while A_c (see eq.1) is the spacecraft specific casualty cross-section, which shall be adopted to be constant at 10m^2 for all risk calculations within this paper (the NASA guidelines [10] require that $A_c \leq 8$m^2 for all uncontrolled re-entries). By definition of the 2σ impact corridor (see Tab.1), and due to integration over the rectangular area instead of the uncertainty ellipse, the impact probability $P_{i,2\sigma}$ will always be 0.911, with less than 9% chance of an impact outside the 2σ rectangular bounds.

7. THE SKYLAB RE-ENTRY

Skylab was launched on 14-May-1973 into a near-circular orbit of 50.0° inclination, with an initial altitude of 434 km which was raised to 441 km in Feb 1974, after the last of three crews had left. There were no major orbit manoeuvres thereafter. Due to an unexpectedly high level of solar activity with the approach of the maximum of solar cycle 21, the 10 year lifetime predicted in early 1974, was significantly shortened, and Skylab re-entered on 11-Jul-1979 at 16:37 UTC, above the Indian Ocean and Australia [2]. Prior to the re-entry, Skylab was re-activated on 06-Mar-1978. Subsequently, residual attitude control capabilities were used to perform an orbit energy management by changing the effective aerodynamic cross-section of the 74 ton compound of length 25.6 m and diameter 6.6 m. The mean area-to-mass ratio A/m could be altered by a factor of 2 between a sun-inertial (SI) high drag, and an end-on-velocity-vector (EOVV) low drag attitude. On 25-Jan-1979 the attempt to prolong orbital lifetime (in an EOVV configuration) was aban-

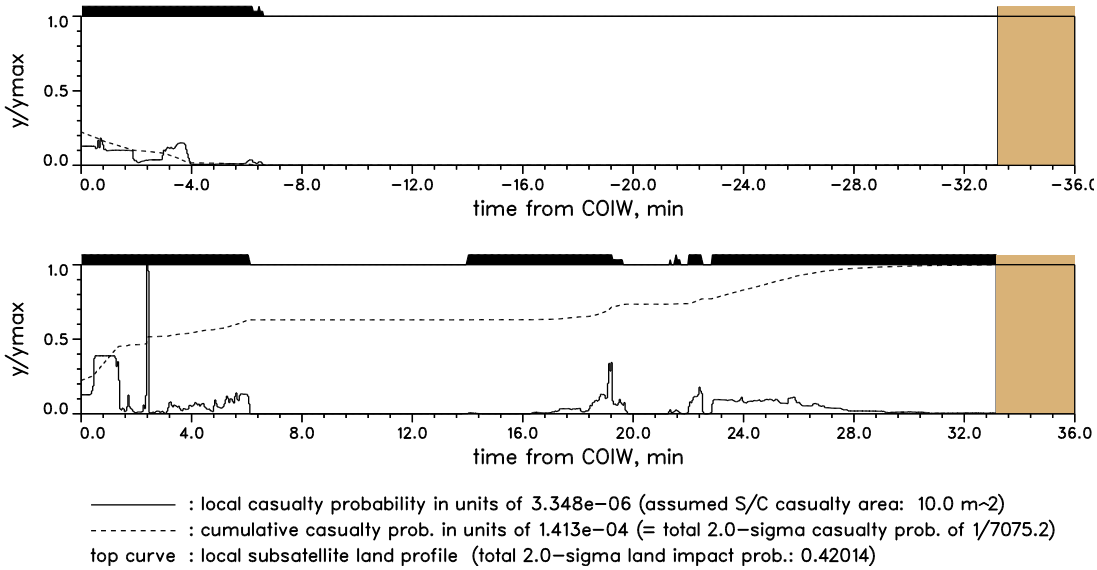

Fig. 6: Salyut-7 re-entry risk distribution along a 2σ ground swath extension of $\pm 16,202$ km (sampled over ± 80 km cross track extension). - Orbit epoch: t_{COIW}-3h. COIW prediction: 1991/02/07 03:50 UTC at $\lambda = -51.0°$ and $\phi = -24.6°$.

doned, and Skylab was left in an SI attitude, which was followed by a torque-equilibrium attitude (TEA) to control the longitude position λ_n of the ascending node of the predicted re-entry groundtrack.

The Skylab re-entry predictions during the last 24 hours of its orbital lifetime were all located on a single groundtrack with an ascending node at the geographical longitude $\lambda_n = 174°$W. Fig.5 shows that this longitude, which was attained by an orbit energy management strategy, results in a re-entry ground swath with a global minimum in mean population density, and hence in mean casualty probability (averaged over one orbit). During the last 24 hours, predictions indicated that the COIW location walked backwards towards the densely populated North America. At T-13h before the predicted entry, the land impact probability was 19.3%, and the casualty probability was 1/31,600. In order to further reduce the risk, Skylab was taken out of its torque-equilibrium attitude (TEA) and put into a tumbling motion at 07:45 UTC on 11-Jul-1979. This led to a drag reduction of about 20%, moving the impact location downtrack by about 1/2 orbit, and placing the COIW right between two successive passes across the densely populated North American landmass. Fig.5 (label "Skylab") shows the corresponding groundtrack pattern, based on TLE data from 10:57 UTC (at T-5.5h). Due to the executed attitude manoeuvre, the probability of land impact was reduced to 16.5%, and the population casualty risk was reduced by almost 25% to 1/40,509. This risk figure corresponds to less than 20% of the global mean casualty risk of 1/7,750 for a reference spacecraft casualty cross section of 10m^2.

The reconstructed impact of Skylab was determined for 11-Jul-1979 at 16:37 UTC, north-east of the Australian city of Esperance, at 32°S and 124°E. Several large fragments could be retrieved from ground, including a water tank, a heat exchanger, an airlock shroud, oxygen bottles, and a film vault (in ascending order, along track).

8. THE SALYUT-7 RE-ENTRY

Salyut-7, a precursor of the Mir space station, was launched on 19-Aug-1982. A week later, its initial near circular orbit of mean altitude 475 km and inclination 51.6° was reached. Following a series of crew visits (Sojus T-5 to T-14) and dockings with supply spacecraft (Progress 13 to 24), the 20 ton Salyut-7 station (with Sojus T-14 attached) was complemented by an unmanned Kosmos-1686 module of the same mass on 02-Oct-1985. After separation and return to Earth of Sojus T-14 on 21-Nov-1985, the Salyut-7/Kosmos-1686 compound of 40 tons mass and 26 m length was left mothballed at 475 km in Aug 1986. From there it started its descent into the atmosphere which led to a final re-entry above South America at 03:45 UTC on 07-Feb-1991.

In contrast with Skylab, Salyut-7 did not have sufficient residual control capability to effectively influence its re-entry time and the resulting groundtrack pattern. For most of its descent period, Salyut-7/K-1686 was in a passive, high drag gravity gradient orientation, with its longitudinal axis close to the local vertical. With increasing air drag, a precession with 10° to 20° coning angle was superimposed. Two days before the predicted re-entry, an attempt was made to re-orientate the Salyut-7 space station into an attitude with reduced air drag, in order to extend the lifetime and shift the probable impact location towards groundtracks with minimised casualty risk. Due to an insufficient remnant of propellant this strategy could not be realised. According to the Russian Mission Control Centre, the Salyut-7/Kosmos-1686 re-entered over Argentina on 07-Feb-1991 at 03:47 UTC. At least 3 major fragments could be retrieved after ground impact.

The geographic longitude of the ascending node of the Salyut-7/Kosmos-1686 re-entry orbit was the vicinity of $\lambda_n \approx 13°$W. According to Fig.5 (label "Salyut-7") such a groundtrack leads to a global maximum of land cover-

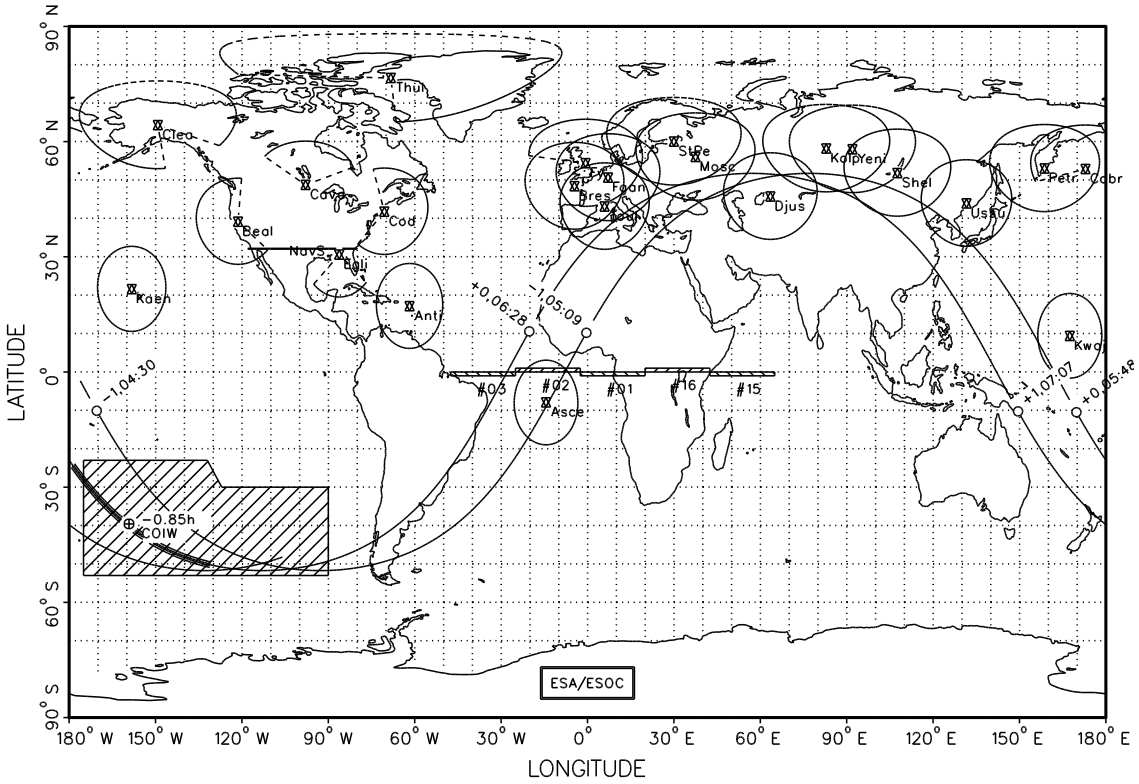

Fig. 7: Mir re-entry groundtrack after a 3-burn de-orbit sequence (9.3 m/s on #15, 10.4 m/s on #16, and 28 m/s on #02). Assumed impact swath extension: $\pm 2,500$ km along track, and ± 100 km cross track (the target impact area is marked).

age, with a risk of casualties close to the global mean. The short-term risk analysis was fairly stable during the last 3 days, and the final casualty probability was estimated to be $P_{c,2\sigma}$ =1/7,050, based of an orbit determination from T-2.77h. This value is close to the global average of 1/7,650 for this orbit inclination of 51.5°, and for the reference spacecraft casualty cross-section of $A_c = 10\text{m}^2$. The corresponding land impact probability is about 42.0%, which is close to the global maximum of 45.0% over a single orbit. Fig.6 shows in more detail that 60% of the casualty risk is compiled during the pass of South America and its densely populated coast line, while another 30% is due to the downrange possibility of a pass across North Africa and Europe.

9. THE MIR RE-ENTRY

The core module of Mir, the successor of the Salyut-7 space station, was launched on 20-Feb-1986. Five more modules were attached between Mar 1987 and Apr 1996. Up to early 2001 several Progress and Soyuz capsules, and a number of Shuttle missions serviced the 135 t space station, which had extensions of 30 m in all three dimensions. On 27-Jan-2001 a specially equipped Progress M1-5 capsule docked with Mir. Following a natural orbital decay to about 215 km mean altitude, the space station was de-orbited in a controlled manner on 23-Mar-2001, following a 3-manoeuvre burn strategy within 4 consecutive orbits, leading to a splash down near $\lambda = -160.0°$ and $\phi = -40.0°$, at 06:00 UTC, well inside the envisaged re-entry zone as shown in Fig.7. With 51.6° Mir had the same orbital inclination as Salyut-7. Moreover, its de-orbit took place on almost the same final groundtrack as the decay of Salyut-7, with the major difference that the phasing of the Mir re-entry position on that orbit was fully controlled and optimised, such that the distance to the nearest land masses was maximised, and the on ground risk was minimised (compare Fig.5, Fig.6 top chart, and Fig.7). Even when assuming an impact footprint of extensions $\pm 2,500$ km along-track and ± 100 km cross-track (which is $\pm 1,000$ km longer than predicted by TsUP), the derived casualty risk according to the previously described assessment procedure was virtually zero. This demonstrates that even large, massive objects can be safely de-orbited, if adequate design and operational provisions are taken (for ISS similar de-orbiting procedures are considered).

10. RELATIVE RISK LEVEL

The risk analysis for uncontrolled re-entries from orbits of 51.5° inclination (e.g. Skylab, Salyut-7, Mir, and ISS), and the long-term, globally averaged risk assessment for such inclinations results in 2σ population casualty probabilities $P_{c,2\sigma}$ which are of the same order of magnitude as the permissible threshold of $P_{c,2\sigma} \leq$1/10,000, which NASA defines [10] for a single uncontrolled re-entry event (assuming a spacecraft casualty cross section of

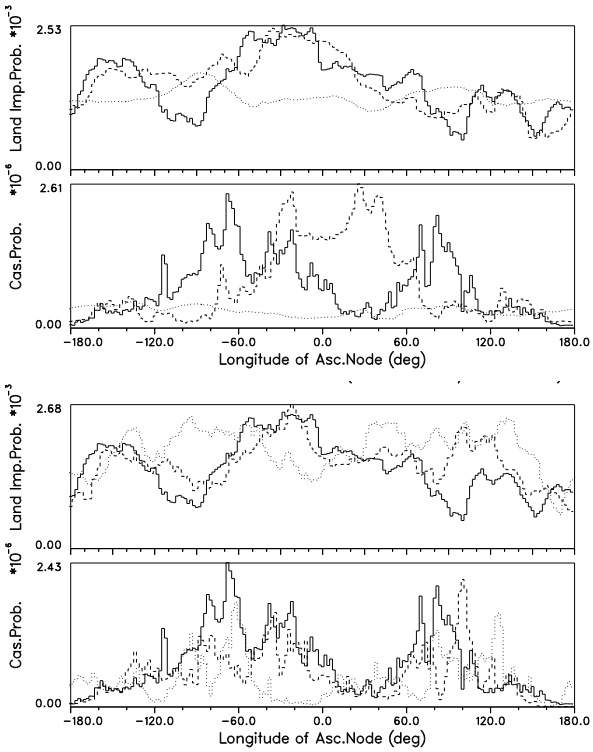

Fig. 4: Land impact, and casualty probability as a function of nodal longitude (2° bins), for orbit inclinations 5.0° (top, dotted), 28.5° (top, dashed), 51.6° (top/bottom, solid line), 65.0° (bottom, dashed), and 98.5° (bottom, dotted).

$A_c \leq 8\text{m}^2$). For the partially controlled natural re-entry of Skylab, this risk level was reduced by more than a factor of 5. In case of the fully controlled de-orbit of Mir, the casualty risk was virtually reduced to zero, by placing the impact footprint in a totally uninhabited area.

If one makes the highly pessimistic assumption that all 17,820 re-entries since Sputnik-1 caused a ground impact with a mean casualty cross-section of 8 m^2, and if one assumes the Earth population of the year 2000 ($6.228 \times 10^{+9}$, corresponding to a global mean population density of 12.2 per km^2), then the cumulated risk of casualties would be 1.7 within 43 years. This risk can be translated into an equivalent personal risk. For a US citizen, the risk to be killed before reaching the age 50 is about 1 in $7 \times 10^{+9}$ due to debris impacts, 1 in 20,000 due to asteroid impacts, 1 in 20,000 due to airplane crashes, 1 in 300 due to homicides, and 1 in 100 due to car accidents. Hence, in spite of the wide public attention which is paid to uncontrolled re-entries of large spacecraft, the associated probability of casualties is several orders of magnitude below the level of day to day risks which are commonly accepted.

11. CONCLUSIONS

A method has been outlined to assess the re-entry risk potential of large, man-made space objects. As part of the analysis the probability of land impact, and the probability of human casualties can be determined, based on empirically justified 2σ bounds of a 2-dimensional impact probability density function along a drift corrected groundtrack. The extension of the assumed 2σ impact dispersion area can be dynamically adjusted as the remaining orbital lifetime diminishes in the course of a re-entry prediction campaign. The risk analysis methods described in this paper were applied to the historic re-entries of Skylab (a 74 ton spacecraft with some residual control capability) and Salyut-7/Kosmos-1686 (a 40 ton spacecraft with no control capability). Also the risk associated with the fully controlled de-orbit of the 135 ton Mir space station on 23-Mar-2001 was analysed, confirming a casualty risk reduction close to zero due to proper selection of the impact footprint.

REFERENCES

[1] Bouslog, S.A., Ross, B.P., and Madden, C.B., *Space Debris Re-Entry Risk Analysis*, AIAA 94-0591, 32nd Aerospace Sciences Meeting, Reno/NV, Jan 10–13, 1994

[2] Dreher, P.E., Little, R.P., and Wittenstein, G., *Skylab Orbital Lifetime Prediction and Decay Analysis*, NASA Technical Memorandum 78308, 1980

[3] Fritsche, B., Roberts, T., Romay, M., Ivanov, M., Grinberg, E., and Klinkrad, H., *Spacecraft Disintegration During Uncontrolled Atmospheric Re-Entry*, proceedings of the Second European Conference on Space Debris, ESA SP-393, pp. 581–586, Darmstadt, 1996

[4] Johnson, N.L., *The Re-Entry of Large Orbital Debris*, IAA 97-6.4.08, 48th IAF Congress, Turino/Italy, Oct 6–10, 1997

[5] Klinkrad, H., *Salyut-7/Kosmos-1686 Re-Entry Prediction Activities at ESOC*, proceedings of an International Workshop on Salyut-7/Kosmos-1686 Re-Entry, ESA SP-345, pp. 17–34, Darmstadt, 1991

[6] Klinkrad, H. (editor), *ESA Space Debris Mitigation Handbook*, rel. 1.0, ESA, Apr 22, 1996

[7] Klinkrad, H., *Evolution of the On-Ground Risk During Uncontrolled Re-Entries*, paper IAA-99-IAA.6.7.05, 50th IAF Congress, Amsterdam/The Netherlands, 1999

[8] Kompaniets, E.P., and Shatrov, Y.T., *Investigation of Application of Concept of Real Risk Level for Choosing Routes of Launch Vehicle Flights and Dropping Areas for Separating Parts*, IAA 97-6.1.01, 48th IAF Congress, Turino/Italy, Oct 6–10, 1997

[9] Tobler, W., Deichmann, U., Gottsegen, J., and Maloy, K., *The Global Demography Project*, Technical Report TR-95-6, National Center for Geographic Information and Analysis, Dept. of Geography, University of California, Santa Barbara/CA, Apr, 1995

[10] Reynolds, R.C., and Loftus, J.P., *A Handbook to Support the NASA Policy to Limit Orbital Debris Generation*, IAA 3.3-93-700, 44th IAF Congress, Graz/Austria, Oct 16–22, 1993

[11] Smith, P.G., *Expected Casualty Calculations for Commercial Space Launch and Reentry Missions*, US Dept. of Transportation/FAA, Advisory Circular 431.35-1, Apr 12, 1999